Calibration of the Radio Neutrino Observatory in Greenland (RNO-G)

Christoph Welling[a,*] **for the RNO-G Collaboration**

(a complete list of authors can be found at the end of the proceedings)

[a]*Dept. of Physics, Enrico Fermi Inst., Kavli Inst. for Cosmological Physics, University of Chicago, Chicago, IL 60637, USA*

E-mail: christophwelling@uchicago.edu

The Radio Neutrino Observatory Greenland (RNO-G) is a radio detector for neutrinos with energies above ~10 PeV. It is currently under construction at Summit Station, Greenland, with 7 out of 35 stations deployed so far. By measuring the radio pulses that are emitted when ultra-high energy neutrinos interact in ice, each station can detect neutrinos over distances of several kilometer and functions as an independent detector. A station consists of a total of 24 antennas, which are divided into a shallow component of 9 logarithmic-periodic dipole antennas near the surface, and a deep component of dipole and slot antennas inside boreholes down to 100m depth. We present an overview of the calibration efforts for RNO-G and show first results of ice property studies, which are crucial for the RNO-G station calibration.

The 38th International Cosmic Ray Conference (ICRC2023)
26 July – 3 August, 2023
Nagoya, Japan

ICRC2023
38th International Cosmic Ray Conference
The Astroparticle Physics Conference

---

*Speaker
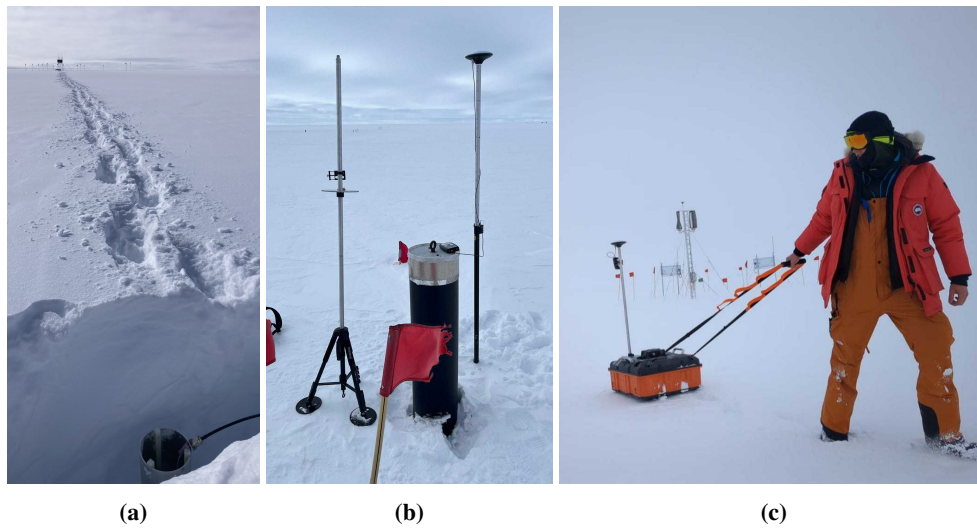
Figure 1: RNO-G calibration measurements in the field: Temporary surface pulser at an RNO-G station (a). GPS survey (b). Survey using ground penetrating radar (c)

1. Introduction

The Radio Neutrino Observatry in Greenland (RNO-G) [1] is a neutrino detector located at Summit Station, Greenland. It aims to detect the first neutrinos at EeV energy scales by measuring the Askaryan radio emission induced when they interact in the ice. Seven out of a total of 35 detector stations have been constructed so far, with each station acting as an independent detector. A station consists of three so-called *strings*, on which antennas are lowered into boreholes at depths up to 100 m. One string, called the *power string*, holds a phased array with four vertically polarized (Vpol) antennas at 100 m depth, two horizontally polarized (Hpol) antennas directly above the phased array, and three more Vpol antennas spaced further up in 20 m intervals. The two *helper strings* are more sparsely instrumented, with two Vpol and one Hpol antennas at a depth of 100 m on each, as well as a calibration pulser. Additionally, nine logarithmic-periodic dipole antennas (LPDAs) are buried just below the surface, six of which point downwards and three upwards. The upwards-facing antennas are used for air shower detection. The detector design is described in more detail in [2].

It has been shown that if RNO-G detects a neutrino, it will be able to also determine its direction and its energy [3, 4], but only if the detector has been well calibrated. This includes the positions of its antennas, the signal chain response and the properties of the ice that is used as a detection medium. In this proceeding we will give an overview over the ongoing calibration efforts for RNO-G.

2. Detector Calibration

The main tools for in-situ calibration of the RNO-G detector are sources of radio signals with known positions and signal properties. We employ several radio pulsers, both permanently and temporarily installed. Furthermore, environmental radio sources are also available to be used for calibration.

Each RNO-G station includes three in-situ radio pulsers: One on each helper string, and one installed at the surface. These pulsers can be operated remotely, allowing for calibration runs any time RNO-G is running, without a field team present. The signals from these in-situ pulsers can be detected by most channels of the station (see Fig.2), though the channels directly next to the pulser usually saturate. Additionally, each field season included calibration measurements where radio pulsers were temporarily installed at varying locations. At each station, radio pulses were transmitted from each cardinal direction by a pulser temporarily buried just below the surface at a distance of ~100 m (Fig.1a). During the 2023 field seasons, the pulsers were triggered on each full second using a GPS unit, which allows to measure not only the differences in propagation time between channels, but also the total propagation time from the pulser. These pulser signals could only be recorded by the station directly next to them, so an additional pulser was temporarily installed on a snow berm near the Summit Mobile Garage (SMG) building, which was observable by multiple stations at the same time, to improve position and timing calibration between stations.

Other radio emitters can be used for calibration as well, if their position is known well enough. An airplane tracker installed on the roof of the MSF building at Summit Station records the transponder signals, which encode the plane's position and altitude, both from commercial airliners and Air National Guard flights to Summit Station, which often fly over the RNO-G array during their landing approach. Radiosonde balloons are launched twice a day from Summit Station as part of the *Integrated Characterization of Energy, Clouds, Atmospheric state, and Precipitation at Summit* (ICECAPS) project and, depending on wind conditions, often fly over the RNO-G array. They emit a continuous wave signal at 403 MHz, and position data from a GPS on board is shared with us by the ICECAPS group. The RNO-G antennas near the surface are also sensitive to galactic noise and solar flares, which is discussed in more detail in [5].

2.1 Timing and Antenna Position

In order to be able to reconstruct the origin of a radio signal detected by RNO-G, the position of each antenna needs to be known precisely to within a few centimeters, as well as the time delays from the signal chain.

After each deployment season, a GPS survey of the positions of each borehole, surface antennas and other station objects, like solar panels and DAQ boxes, was carried out. Using a reference GPS antenna installed on the Mobile Science Facility (MSF) at Summit Station, a precision of a few centimeters can be achieved using post-processing kinematics (PPK). The GPS surveying has proven tricky, due to the degrading satellite coverage at northern latitudes. The depths of the antennas was recorded during deployment using a tape measure attached to each *string*.

These measurements serve as a starting point, but a more precise calibration is necessary to account for GPS uncertainty, movement of the antennas while lowering, and a possible tilt in the holes. This is done by cross-correlating the waveforms of pulser signals recorded in different channels to determine the time offset between them. The time offsets are corrected for the time delays introduced by the signal chain, which have been precisely measured prior to deployment. The remaining time differences are due to different propagation times from the pulser to the antennas and can be used to constrain their positions. However, the index of refraction profile of the upper ~100 m of the ice sheet, called the firn, is not well constrained. Therefore, constraining the antenna positions and the index of refraction profile of the firn are highly interlinked.
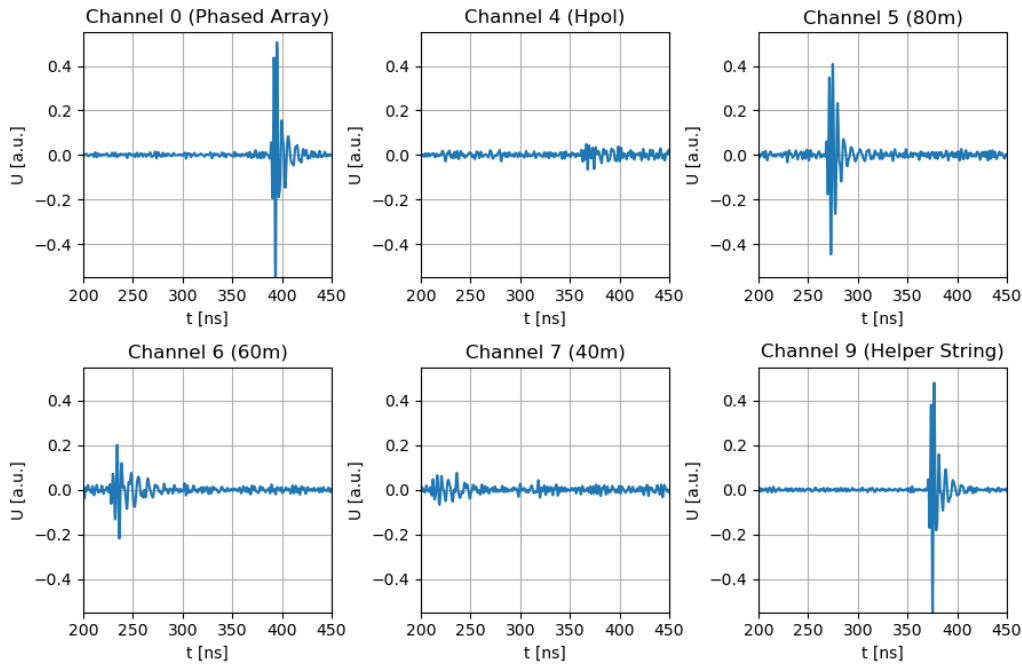
Figure 2: Signals from the pulser on one of the helper strings recorded by an RNO-G station. Channel 0 is one of the four antennas that make up the phased array. Channel 4 is one of the horizontally polarized antennas on the *power string*. Channels 5, 6, and seven are vertically polarized antennas on the *power string* at 80 m, 60 m and 40 m, respectively. Channel 9 is one of the vertically polarized antennas on a *helper string*.

## 2.2 Antenna and Signal Chain Response

Signals recorded by an antenna on one of the *strings* is fed into a low-noise amplifier (LNA) and converted into an optical signal which is sent upwards via RF over fiber (RFoF), where it is converted back into a voltage and amplified again, before being fed into the digitizer. To reconstruct the radio signal that was received at the antenna from the signal arriving at the digitizer, the effect that each element in this chain has on the signal has to be understood. The signal responses of the receiving antennas have been simulated using final difference time domain (FDTD) simulations [2]. The signal chain from the antennas to the digitizer, as well as the output of the pulse generators, have been characterized with a Vector Network Analyzer before installation. In-situ calibration is still necessary, to verify these measurements and account for temperature dependence, faulty fiber connections, or possible damage during deployment. This is done by comparing the measured signals from the in-situ pulsers to what is expected from simulations. An example of this is shown in Fig.3: Up to ~400 MHz, the channels perform as expected, but there is some deviation at higher frequencies, which is being investigated.

2.3 Digitizer Calibration

After passing through the analog signal chain, the signal is digitized and converted into a series of integers, called *ADC counts*, which are written onto an SD card. For data analysis, these ADC counts need to be converted back into voltages, requiring the ADC to be recalibrated regularly. This is done by applying a bias voltage to the ADC input and varying it to scan over the ADC's dynamic
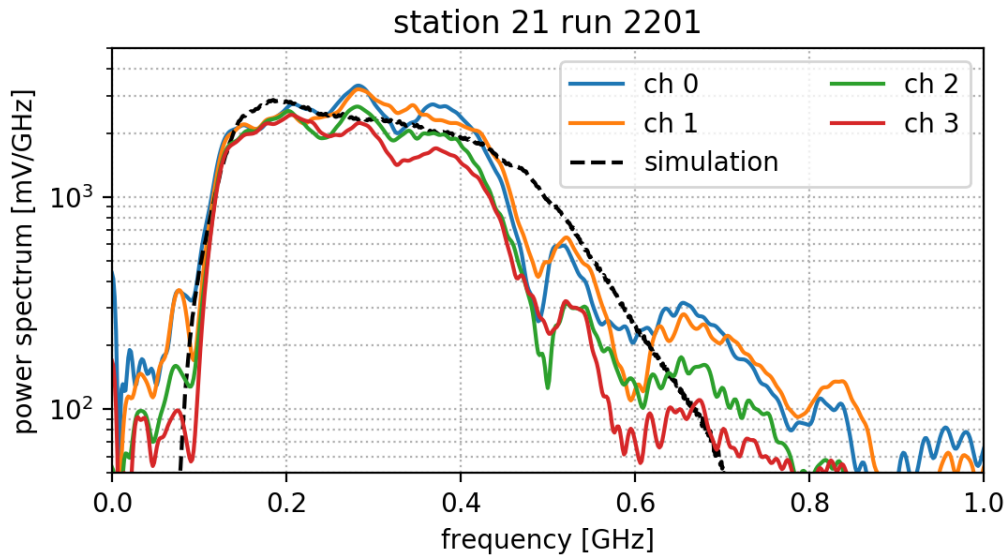
Figure 3: Spectrum of the signal from an in-situ pulser recorded by the phased array channels of RNO-G station 21, along with the simulated spectrum, rescaled to match the measurements.
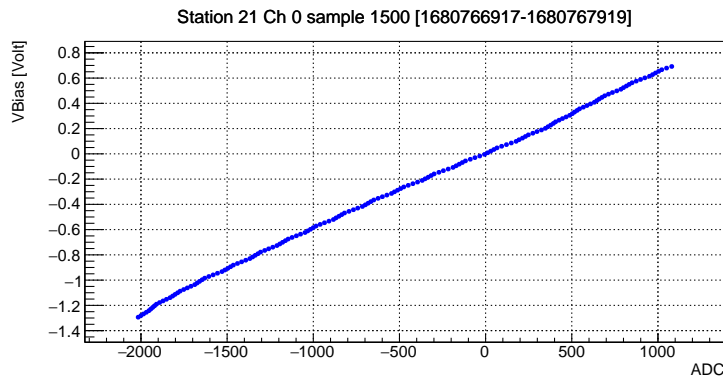
Figure 4: Example of a digitizer calibration, showing the relation between the ADC count and the bias voltage that is applied to the ADC.

range. From this, each ADC count can be matched to a corresponding voltage, which is shown in Fig. 4. The relationship between bias voltage and ADC count is roughly linear, but some deviations require a more careful calibration. Additionally, each sample has to be characterized individually, and temperature effects have to be taken into account as well. In the future, this measurement will be performed automatically in regular intervals, to ensure a good calibration at all times.

3. Ice Properties

A radio signal emitted from a neutrino induced particle cascade will have to cross up to several kilometers of ice before reaching the detector. Because of this, understanding the ice at Summit Station is essential in order to be able to reconstruct a neutrino from the detected radio signals.

During each field season, radioglaciological measurements were performed in order to characterize properties of the ice that makes up the detector.

3.1 Attenuation Length

The attenuation length was measured in 2021 by transmitting radio pulses downward into the ice and recording their reflections off the bedrock [6, 7]. By comparing the strength of the transmitted and received signals, the mean attenuation length over the full ice depth can be calculated. From this, the attenuation length as a function of depth is calculated, based on data from the nearby GISP2 and GRIP boreholes. The attenuation length over the upper 1.5 km, the region from where most neutrino detections are to be expected, is roughly constant with a value around 900 m. An additional estimate of the depth dependence of the attenuation length can be made using reflections off layers within the ice sheet [7]. Assuming that, on average, the reflectivity of these internal layers is not dependent on depth, the change in the power of the reflected signals with layer depth can be attributed to attenuation. While this method has a large uncertainty, it confirms our measurement of the attenuation length of the upper part of the ice sheet.

3.2 Index of Refraction

The index of refraction in the upper part of the ice sheet, called the firn, increases from a value of ~ 1.3 near the surface to 1.78, as the accumulated snow is compressed into solid ice. This causes the paths of radio signals to bend downwards in the firn, and requires a precise knowledge of the firn index of refraction profile in order to be able to reconstruct their arrival directions. In simulation studies, the index of refraction profile is often modelled with an exponential function, because in this case, an analytic solution to the raytracing problem exists, which greatly speeds up simulations [8]. The real index of refraction profile is more complex however. A model based on measurements of the firn density, shows a better agreement with measured signal propagation times from radio pulsers, though significant discrepancies still remain [9].

Just like the antenna position, the firn index of refraction profile can be constrained by the signal propagation times from a pulser to the RNO-G antennas.

Another way to measure the index of refraction profile is through a ground penetrating radar (GPR) system, which was used in the 2023 field season (Fig.1c). If the depth of a reflector in the ice is known, the average index of refraction of the ice above it can simply be calculated from the timing of the radar echo. If the target depth is not known, the index of refraction can be measured using the radar echo time as the horizontal distance from the target is increased [10]. Useful targets for this are the antennas of an RNO-G station (which will also help with the antenna position calibration).

Below the firn, the index of refraction is constant and no refraction occurs. However, knowing the precise value of the index of refraction is still necessary, as it determines the Cherenkov angle in the medium, which is important to reconstruct the direction of a detected neutrino [3]. The bulk ice index of refraction was measured using reflections from layers in the ice. Most of these reflective layers are caused by changes in the conductivity of the ice. By matching radio echos to ice conductivity data from the GISP2 and GRIP ice cores we were able to precisely measure the index of refraction of the bulk ice to be $n = 1.778 \pm 0.006$[11].

3.3 Additional Glaciological Measurements

Glacial ice has been shown to have birefringent properties due to the alignment of the ice crystals caused by pressure or sheer stress. We compared the propagation times of the bedrock echo for different antenna orientations, and found no dependence on signal polarization, and therefore no significant birefringence [7]. It should be noted though, that birefringence effects are expected to be stronger for a radio signal moving horizontally through the ice than for one moving vertically, if the ice flow is slow, as is the case at Summit Station.

The internal reflectors inside the ice sheet have been proposed as a potential source of background, if they reflect radio signals from air showers that impact the ice surface [12]. We measured the reflectivity of these reflectors, which was between -70 dB and -60 dB, ruling them out as a source of background. However, because of amplifier saturation, we could only probe reflectors deeper than 200 m.

4. Conclusion

The Radio Neutrino Observatory in Greenland is an experiment to detect the Askaryan emission from UHE neutrinos interacting in the ice around Summit Station, Greenland. Seven out of a total of 35 planned detector stations have been constructed so far, and calibration efforts are ongoing. Individual components that make up the signal chains of each detector station have been carefully characterized before deployment. Three in-situ calibration pulsers are installed at each station and can be operated remotely any time RNO-G is running. Additionally, every field season included calibration measurements using pulsers temporarily installed at various points around the stations and RF signals from airplanes and radiosonde balloons with known positions are available. These are used to calibrate the positions of the radio antennas as well as the response of the signal chain.

The ice, which forms the detection medium for RNO-G, has been characterized by radioglaciological measurements. The attenuation length and the index of refraction of the bulk ice have been measured using radio echos off the bedrock and reflective layers in the ice. Additionally, constraints on birefringent properties of the ice have been placed and the reflectivity of deep ice layers has been measured. These efforts will continue over the following years to ensure RNO-G is well calibrated and able to reconstruct neutrino events when it finds them.

References

[1] **RNO-G** Collaboration, J. A. Aguilar *et al. JINST* **16** no. 03, (2021) P03025. [Erratum: JINST 18, E03001 (2023)].

[2] J. A. Aguilar and others. *PoS* **ICRC2021** (2021) 1058.

[3] I. Plaisier, S. Bouma, and A. Nelles *Eur. Phys. J. C* **83** no. 5, (2023) 443.

[4] J. A. Aguilar *et al. Eur. Phys. J. C* **82** no. 2, (2022) 147.

[5] J. A. Aguilar and others. *PoS* **ICRC2023** (2023) .

[6] J. A. Aguilar, P. Allison, J. J. Beatty, D. Besson, A. Bishop, O. Botner, S. Bouma, S. Buitink, M. Cataldo, B. A. Clark, and et al. *Journal of Glaciology* **68** no. 272, (2022) 1234–1242.

[7] J. A. Aguilar *et al. submitted to Journal of Glaciology* (12, 2022) .

[8] C. Glaser *et al. Eur. Phys. J. C* **80** no. 2, (2020) 77.

[9] C. Deaconu, A. G. Vieregg, S. A. Wissel, J. Bowen, S. Chipman, A. Gupta, C. Miki, R. J. Nichol, and D. Saltzberg *Phys. Rev. D* **98** no. 4, (2018) 043010.

[10] J. S. Rønning *Near Surface Geophysics* **21** no. 3, (2023) 171–181.

[11] J. A. Aguilar *et al. Submitted to Cryosphere* (2023) .

[12] S. De Kockere, K. de Vries, and N. van Eijndhoven *PoS* **ICRC2021** (2021) 1032.

Full Author List: RNO-G Collaboration

J. A. Aguilar[1], P. Allison[2], D. Besson[3], A. Bishop[10], O. Botner[4], S. Bouma[5], S. Buitink[6], W. Castiglioni[8], M. Cataldo[5], B. A. Clark[7], A. Coleman[4], K. Couberly[3], P. Dasgupta[1], S. de Kockere[9], K. D. de Vries[9], C. Deaconu[8], M. A. DuVernois[10], A. Eimer[5], C. Glaser[4], T. Glüsenkamp[4], A. Hallgren[4], S. Hallmann[11], J. C. Hanson[12], B. Hendricks[14], J. Henrichs[11,5], N. Heyer[4], C. Hornhuber[3], K. Hughes[8], T. Karg[11], A. Karle[10], J. L. Kelley[10], M. Korntheuer[1], M. Kowalski[11,15], I. Kravchenko[16], R. Krebs[14], R. Lahmann[5], P. Lehmann[5], U. Latif[9], P. Laub[5], C.-H. Liu[16], J. Mammo[16], M. J. Marsee[17], Z. S. Meyers[11,5], M. Mikhailova[3], K. Michaels[8], K. Mulrey[13], M. Muzio[14], A. Nelles[11,5], A. Novikov[19], A. Nozdrina[3], E. Oberla[8], B. Oeyen[18], I. Plaisier[5,11], N. Punsuebsay[19], L. Pyras[11,5], D. Ryckbosch[18], F. Schlüter[1], O. Scholten[9,20], D. Seckel[19], M. F. H. Seikh[3], D. Smith[8], J. Stoffels[9], D. Southall[8], K. Terveer[5], S. Toscano[1], D. Tosi[10], D. J. Van Den Broeck[9,6], N. van Eijndhoven[9], A. G. Vieregg[8], J. Z. Vischer[5], C. Welling[8], D. R. Williams[17], S. Wissel[14], R. Young[3], A. Zink[5]

[1] Université Libre de Bruxelles, Science Faculty CP230, B-1050 Brussels, Belgium

[2] Dept. of Physics, Center for Cosmology and AstroParticle Physics, Ohio State University, Columbus, OH 43210, USA

[3] University of Kansas, Dept. of Physics and Astronomy, Lawrence, KS 66045, USA

[4] Uppsala University, Dept. of Physics and Astronomy, Uppsala, SE-752 37, Sweden

[5] Erlangen Center for Astroparticle Physics (ECAP), Friedrich-Alexander-Universität Erlangen-Nürnberg, 91058 Erlangen, Germany

[6] Vrije Universiteit Brussel, Astrophysical Institute, Pleinlaan 2, 1050 Brussels, Belgium

[7] Department of Physics, University of Maryland, College Park, MD 20742, USA

[8] Dept. of Physics, Enrico Fermi Inst., Kavli Inst. for Cosmological Physics, University of Chicago, Chicago, IL 60637, USA

[9] Vrije Universiteit Brussel, Dienst ELEM, B-1050 Brussels, Belgium

[10] Wisconsin IceCube Particle Astrophysics Center (WIPAC) and Dept. of Physics, University of Wisconsin-Madison, Madison, WI 53703, USA

[11] Deutsches Elektronen-Synchrotron DESY, Platanenallee 6, 15738 Zeuthen, Germany

[12] Whittier College, Whittier, CA 90602, USA

[13] Dept. of Astrophysics/IMAPP, Radboud University, PO Box 9010, 6500 GL, The Netherlands

[14] Dept. of Physics, Dept. of Astronomy & Astrophysics, Penn State University, University Park, PA 16801, USA

[15] Institut für Physik, Humboldt-Universität zu Berlin, 12489 Berlin, Germany

[16] Dept. of Physics and Astronomy, Univ. of Nebraska-Lincoln, NE, 68588, USA

[17] Dept. of Physics and Astronomy, University of Alabama, Tuscaloosa, AL 35487, USA

[18] Ghent University, Dept. of Physics and Astronomy, B-9000 Gent, Belgium

[19] Dept. of Physics and Astronomy, University of Delaware, Newark, DE 19716, USA

[20] Kapteyn Institute, University of Groningen, Groningen, The Netherlands

Acknowledgments